Journal of the European Ceramic Society **12** (1993) 3–13

Tensile Dynamic and Static Fatigue Relations for a HIPed Silicon Nitride at Elevated Temperatures

Chih-Kuang Jack Lin, Michael G. Jenkins* & Mattison K. Ferber
Metals and Ceramics Division, Oak Ridge National Laboratory, Oak Ridge, TN 37831-6064, USA

(Received 7 July 1992; accepted 16 December 1992)

Abstract

Dynamic and static fatigue behavior of a hot-isostatically pressed (HIPed) silicon nitride was investigated at 1150, 1260 and 1370°C. Uniaxial tensile tests were conducted over ranges of constant stresses and constant stress rates. Correlation of stress–life relations between static and dynamic fatigue results was evaluated and failure modes were determined as functions of temperature, stress and stress rate. At 1150°C the static and dynamic fatigue failures were controlled by a slow crack growth mechanism for all stresses and stress rates. Creep rupture was the dominant failure mechanism in static loading at 1260 and 1370°C. A transition in the dominant failure mechanism in dynamic fatigue at 1260 and 1370°C occurred at a stress rate of 10^{-2} MPa/s. Slow crack growth was the dominant failure mechanism with stress rates $> 10^{-2}$ MPa/s while creep rupture was the governing mechanism for the failure at stress rates $\leq 10^{-2}$ MPa/s.

Das dynamische und statische Ermüdungsverhalten heiß-isostatisch-gepreßten (HIPed) Siliziumnitrids wurde bei 1150, 1260 und 1370°C untersucht. Einachsige Zugversuche wurden für verschiedene Spannungs- und Dehnungsraten durchgeführt. Eine Korrelation der Spannungs–Lebensdauer-Beziehung zwischen den Ergebnissen aus statischen und dynamischen Ermüdungversuchen wurde bestimmt und die Versagensarten als Funktion der Temperatur, Spannung und Spannungsrate ermittelt. Das dynamische und statische Ermüdungsversagen bei 1150°C wurde für alle Spannungen und Spannungsraten durch ein langsames Rißwachstum bestimmt. Kriechbruch war der dominierende Versagensmechanismus für statische Belastung bei 1260 und 1370°C. Im dynamischen Ermüdunversuch trat bei 1260 und 1370°C ein Übergang bezüglich des dominierenden Versagensmechanismuses bei einer Spannungsrate von 10^{-2} MPa/s auf. Für Spannungsraten $> 10^{-2}$ MPa/s war das langsame Rißwachstum der bestimmende Versagensmechanismus, während für Spannungsraten $\leq 10^{-2}$ MPa/s Kriechbruch dominierte.

Le comportement à la fatigue statique et dynamique de nitrure de silicium comprimé isostatiquement à chaud (HIPpèd) a été étudié à 1150, 1260 et 1370°C. Des tests de traction uniaxiale ont été effectués dans une gamme de contraintes fixes et de vitesses de mise sous contrainte. On a évalué la corrélation des relations contrainte–durée de vie pour les résultats de fatigue statique et de fatigue dynamique et les modes de fracture ont été déterminés selon la température, la contrainte et la vitesse de mise sous contrainte. A 1150°C, la fracture en fatigue statique et dynamique est contrôlée par un mécanisme de croissance lente des fissures quelles que soient les contraintes et les vitesses de mise sous contrainte. La rupture en fluage est le mécanisme dominant d'endommagement pour une charge statique à 1260 et 1370°C. On observe une transition du mécanisme dominant d'endommagement, qui correspond à une vitesse de mise sous contrainte de 10^{-2} MPa/s, pour les essais de fatigue dynamique à 1260 et 1370°C. La croissance lente des fissures est le mécanisme prédominant aux vitesses de mise sous contrainte $> 10^{-2}$ MPa/s tandis que la rupture en fluage gouverne l'endommagement aux vitesses $\leq 10^{-2}$ MPa/s.

1 Introduction

Ceramic materials offer significant potential for use in structural components of advanced heat engines. To be successful in such structural applications, these materials must provide adequate reliability and long-term strength durability under severe thermal and mechanical loading conditions. Successful designs require comprehensive evaluation of

* Present address: Department of Mechanical Engineering, University of Washington, Seattle, WA 98195, USA.

Journal of the European Ceramic Society 0955-2219/93/$6.00

mechanical and thermal properties under various modes of loading at elevated temperatures where fatigue and creep resistances are major concerns for long-term performance of these structural ceramics.

Creep rupture and slow crack growth (SCG) are typical failure mechanisms in ceramics under long-term loading at elevated temperatures.[1] For creep rupture, failure is usually associated with bulk deformation from extensive nucleation, growth, and coalescence of cavities and microcracks as a result of such creep processes as diffusion or viscous flow. Alternatively, SCG generally occurs by the extension of pre-existing flaws to final, critical sizes. However, localized creep damage in the vicinity of the crack tip may occur in the SCG regime under certain conditions. Both SCG and creep rupture processes are time, temperature and stress dependent.

Silicon nitride ceramics have been the prime candidate materials for advanced heat engine components, because of their high specific strengths and good thermal shock resistances.[2,3] Although creep rupture and elevated-temperature slow crack growth of silicon nitride have been investigated in numerous studies (e.g. Refs 4–15), most of these studies have focused mainly on hot-pressed or gas-pressure sintered silicon nitrides with high volume fractions ($\sim$10 vol.%) of secondary phase contents (MgO, Y_2O_3, Al_2O_3, etc.). Fatigue and creep properties in ceramics are influenced by microstructures which are dependent on processing method, and type and amount of additives.[16–19] Hot-isostatic pressing (HIP) can produce complex-shaped ceramic components of near-net shape. In addition, it can also generate fully dense materials using low amounts of densification aids, e.g. yttria, thus decreasing the volume fraction of secondary phase and improving the elevated-temperature properties. Although HIPed silicon nitrides exhibit excellent short-term strength at elevated temperatures, they are susceptible to SCG and creep rupture which can limit their long-term reliability.[7,8,20] Therefore, it is essential to gain a detailed understanding of the creep and fatigue properties of HIPed silicon nitrides at elevated temperatures representative of projected service conditions.

The purpose of this study was to empirically characterize dynamic and static fatigue behavior of a HIPed silicon nitride in the elevated-temperature regime of advanced heat engine designs. The major part of this investigation was directed toward the dynamic fatigue behavior and its relation with static fatigue results. Tensile test results at 1150–1370°C at constant stresses and constant stress rates are presented. Stress–life relations in static fatigue and strength–stress rate relations in dynamic fatigue are discussed in terms of temperature sensitivity. Direct comparisons between dynamic and static fatigue results provide insight into the failure mechanisms of HIPed silicon nitride at elevated temperatures. These include the evaluation of the applicability of a slow crack growth model to correlate dynamic and static fatigue properties. In addition, fractographic analysis for determining the key features of failure modes is described. In particular, whether the failure of this material for selected testing stress—temperature conditions is controlled by SCG, creep rupture, or a combination of both will be examined.

2 Material and Experimental Procedure

2.1 Material and specimen geometry

The specimens tested in this study were fabricated from a commercial HIPed silicon nitride designated PY6 (GTE Laboratories, Inc., Waltham, Massachusetts, USA, 1989–1990 vintage) which contained $\sim$6 wt% yttrium oxide as the sintering aid. Microstructurally, this ceramic contained 1–6 μm long acicular β-silicon nitride grains surrounded by nominally equiaxed β-silicon nitride grains 0·1–1·0 μm in diameter. The secondary phases at the grain boundaries and 'triple-point' grain junctions were composed primarily of an amorphous to partially crystallized yttrium silicate. Uniaxial tensile testing of ceramics has been recognized as the most feasible method for obtaining valid elevated-temperature mechanical properties data for engineering design purposes.[21] Uniform-gage section tensile specimens with the geometry shown in Fig. 1 were used to perform both static and dynamic fatigue tests. Specimens were machined to the final dimensions from HIPed rods 160 mm long and 20 mm in diameter. Typical gage section surface finishes of R_a (arithmetic average) $\approx$ 0·4–0·6 μm were determined using a diamond stylus surface profilometer.

2.2 Test setup and procedure

All fatigue tests were conducted on commercial electromechanical testing machines equipped with commercial self-aligning hydraulic couplers to minimize bending moments. Percentage bending was measured following the procedure detailed elsewhere[22] using strain-gaged specimens at room temperature to ensure that minimum bending was imposed at the lower loads employed during the static fatigue tests. Generally, the maximum bending at the applied stress levels was $\leq$3% of the uniaxial tensile stress. Compact two-zone resistance-heated furnaces capable of maximum temperatures of 1650°C were used to generate the testing temperatures. Load was transferred to the button heads of the specimens through water-cooled grips located

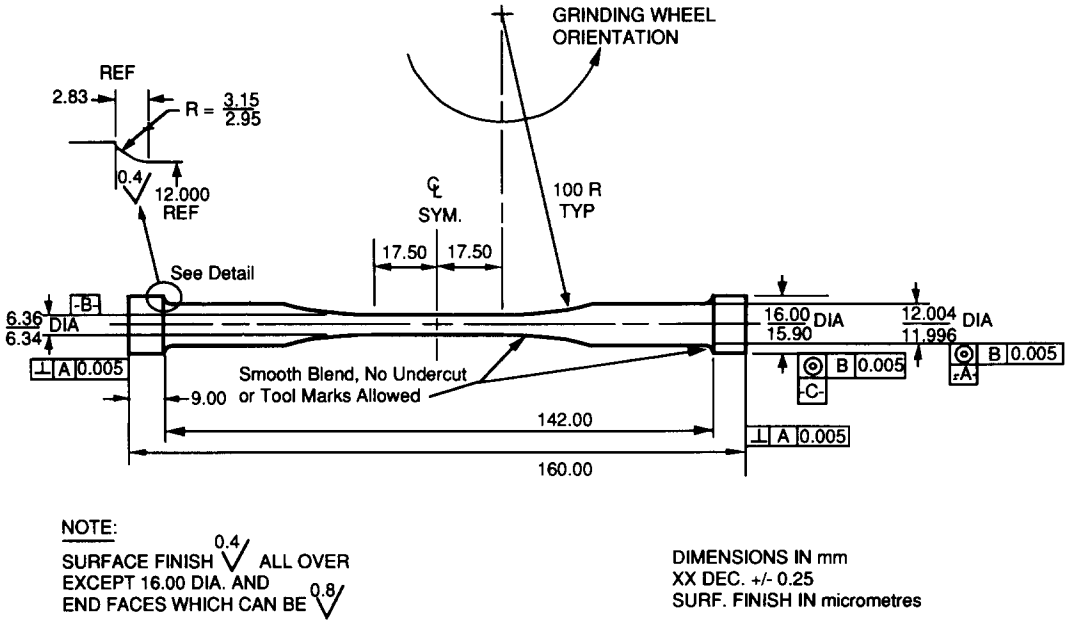

Fig. 1. Geometry of the tested specimens.

outside the furnace. Tensile strains were measured over 25-mm gage lengths with direct-contact extensometers employing remote capacitance sensors and SiC contact probes.

Both static and dynamic fatigue tests were carried out at 1150, 1260 and 1370°C in ambient air. In the static fatigue tests, reported elsewhere,[20] specimens were tested to failure under constant tensile loads with concurrent measurements of the time-dependent strains. In the dynamic fatigue tests, specimens were failed at various stress rates: $3{\cdot}7 \times 10^{1}$, 10^{0}, 10^{-1}, 10^{-2}, 10^{-3} and 10^{-4} MPa/s. Stress–strain curves were also recorded for each dynamic fatigue test so as to monitor the progress of macroscopic deformation.

3 Results and Discussion

3.1 Slow crack growth model

For most ceramics, the subcritical crack growth can be expressed by the following power law relation:[23]

$$V = \mathrm{d}a/\mathrm{d}t = AK_{\mathrm{I}}^{N} = A(Y\sigma\sqrt{a})^{N} \qquad (1)$$

where V is the crack growth rate, a is the crack size, t is time, A and N are assumed material constants, K_{I} is the Mode I stress intensity factor, Y is a geometric factor, and σ is the applied stress. Note that crack growth rates in ceramics are thermally activated processes.

The time to failure, t_{sf}, is the time required for the initial flaw to grow to critical size under a constant applied stress, σ_{a}, and can be approximated by integrating eqn (1) such that:[24]

$$t_{\mathrm{sf}} = BS_{\mathrm{i}}^{N-2}\sigma_{\mathrm{a}}^{-N} \qquad (2)$$

where $B = 2/[AY^{2}(N-2)K_{\mathrm{Ic}}^{N-2}]$, S_{i} is the inert strength, and K_{Ic} is the plane strain fracture toughness.

In a similar approach, the fracture strength, S_{f}, for a specimen under a constant stress rate, $\dot{\sigma}$, can be derived from eqn (1) as the following approximation:[24]

$$S_{\mathrm{f}}^{N+1} = B(N+1)S_{\mathrm{I}}^{N-2}\dot{\sigma} \qquad (3)$$

Equation (3) provides an indication of the stress rate dependence of strength whereby fracture strength increases with increasing stress rate as the crack or crack-like flaw has less time to extend.

The time to failure, t_{df}, for a constant applied stress rate, $\dot{\sigma}$, can also be related to t_{sf}, such that:

$$t_{\mathrm{df}} = (N+1)t_{\mathrm{sf}} \qquad (4)$$

when the applied stress, σ_{a}, for constant stress loading is equal to the fracture strength, S_{f}, under a constant stress rate, $\dot{\sigma}$. Therefore, a simple power law relation such as that described in eqn (1) can be used to predict the failure time of either static or dynamic fatigue given one of the failure times, if both failure modes are dominated by SCG. The crack growth exponent, N, can be determined from static fatigue results or dynamic fatigue results using eqn (2) or (3), respectively.

3.2 Static fatigue behavior

Results of the static fatigue tests at 1150, 1260 and 1370°C are shown in Fig. 2 as a plot of $\log \sigma_{\mathrm{a}}$ versus $\log t_{\mathrm{sf}}$ where each data point represents a single test. As indicated in Fig. 2, t_{sf} decreases with an increase in σ_{a} at each testing temperature. Linear regression analyses of the data points in failed static fatigue specimens provided estimates of N as 22 at 1150°C and 6·4 at 1260 and 1370°. Static fatigue susceptibility increased with increasing temperature from

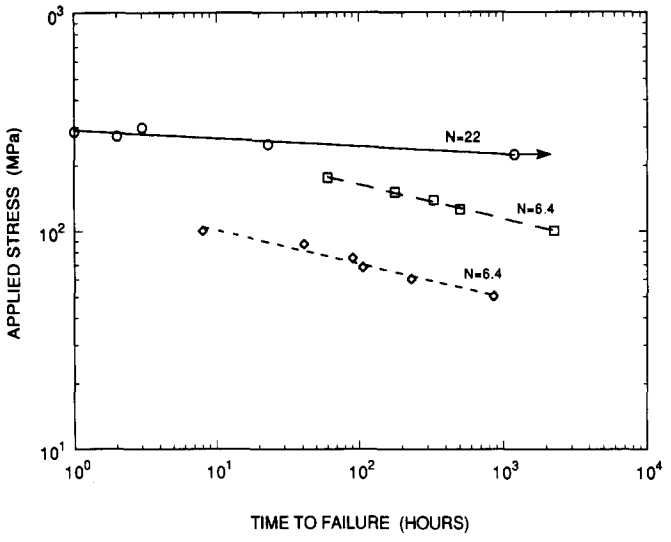

Fig. 2. Tensile static fatigue results of PY6 silicon nitride at (○) 1150, (□) 1260 and (◇) 1370°C. The solid and dashed lines represent the best fit of the experimental data (excluding the run-out point with $\sigma_a = 225$ MPa at 1150°C, indicated by an arrow).

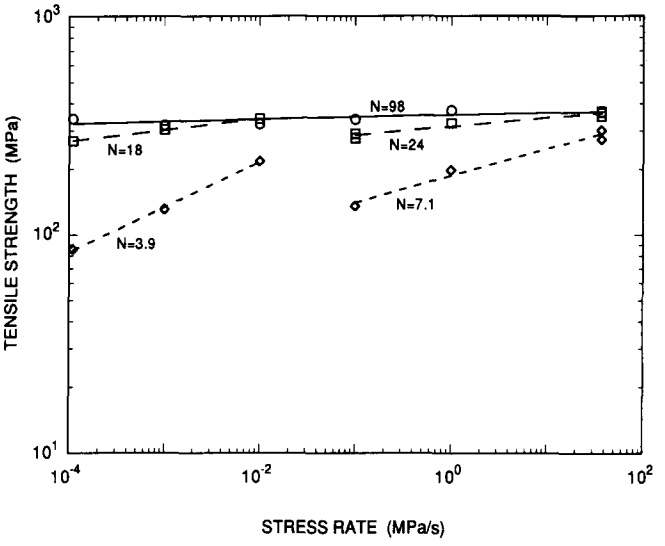

Fig. 3. Tensile dynamic fatigue results of PY6 silicon nitride at (○) 1150, (□) 1260 and (◇) 1370°C. The solid and dashed lines represent the best fit of the experimental data.

1150 to 1260°C as the value of N decreased from 22 to 6·4. However, static fatigue susceptibility did not differ significantly at temperatures greater than 1260°C as the values of N at 1260 and 1370°C were equal.

The difference in the values of N in the temperature range 1150 to 1370°C also implies that the failure mechanisms of static fatigue vary with temperature. It has been reported previously[20] that SCG was the dominant failure mechanism, as indicated by the high value of N at 1150°C, and creep damage was responsible for the failure at temperatures of 1260 and 1370°C, as indicated by lower N values. Furthermore, because the subcritical crack extension in specimens tested at 1150°C was presumably controlled by K_I, the failures at 1150°C were classified as stress controlled. On the other hand, at 1260 and 1370°C, the creep-induced relaxation of crack-tip stresses precluded failure via the stress-controlled mechanism. In this case, fracture resulted when the strain associated with the creep damage reached a critical value described by the Monkman–Grant relation (i.e., strain-controlled fracture). Detailed discussion of the stress and temperature sensitivities of the secondary (or minimum) creep rate and other creep properties has also been addressed previously.[20]

3.3 Dynamic fatigue behavior

Figure 3 illustrates the dynamic fatigue results as log–log plots of S_f versus $\dot{\sigma}$ at three different temperatures. These results show a general trend of decreasing fracture strength with decreasing stress rate at 1150°C. At 1260 and 1370°C this trend is also present in two regions: stress rates $>$ and $\leq$ 10^{-2} MPa/s, respectively. However, the failure stresses for 10^{-2} MPa/s at 1260 and 1370°C exceeded the failure stresses for the nearest higher applied stress rate at each corresponding temperature. For stress rates $> 10^{-2}$ MPa/s the values of N were estimated as 24 at 1260°C and 7·1 at 1370°C. The N values for stress rates $\leq 10^{-2}$ MPa/s were estimated as 18 and 3·9 at 1260 and 1370°C, respectively. No such transition in the dynamic fatigue curve at 1150°C was observed for selected stress rates in the current study, and the value of N was determined as 98. This high value of N indicated that this material was not very sensitive to dynamic fatigue at 1150°C, as the strength did not substantially decrease with decreasing stress rate. However, at 1260 and 1370°C, the N values became much less with increased susceptibility to dynamic fatigue. An earlier study[25] of a similar material also reported decreasing N with increasing temperature in which the values of N in flexural dynamic fatigue tests were determined as ∞ at room temperature, 73 at 1000°C, 30 at 1200°C, and 8·8 at 1400°C.

The shift of N values in dynamic fatigue curves at 1260 and 1370°C implies the change of dominant failure mechanism from SCG to creep rupture with decreasing stress rate. A similar transition behavior has been observed in a HIPed SiC whisker-reinforced silicon nitride composite at 1300°C.[26] The apparent change in failure mechanism is also evident in the stress–strain curves from dynamic fatigue tests as shown in Fig. 4. At all stress rates at 1150°C the stress–strain curves exhibited substantial linear portions (with nearly identical slopes) becoming nonlinear just prior to failure (see Fig. 4(a)). This shift from linear to nonlinear stress–strain behavior may reflect compliance changes resulting from SCG. Similar linear to nonlinear stress–strain behavior (with nearly identical slopes in linear portions) was also observed at 1260 and 1370°C at stress rates $> 10^{-2}$ MPa/s (see Fig. 4(b) and (c)). However, creep

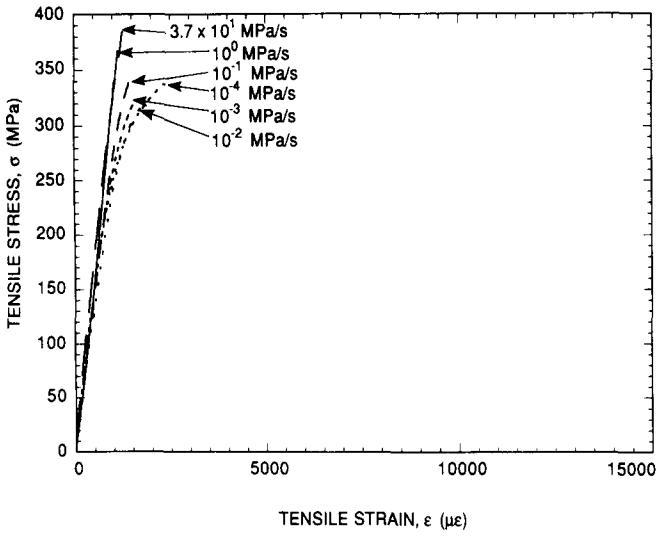

(a)

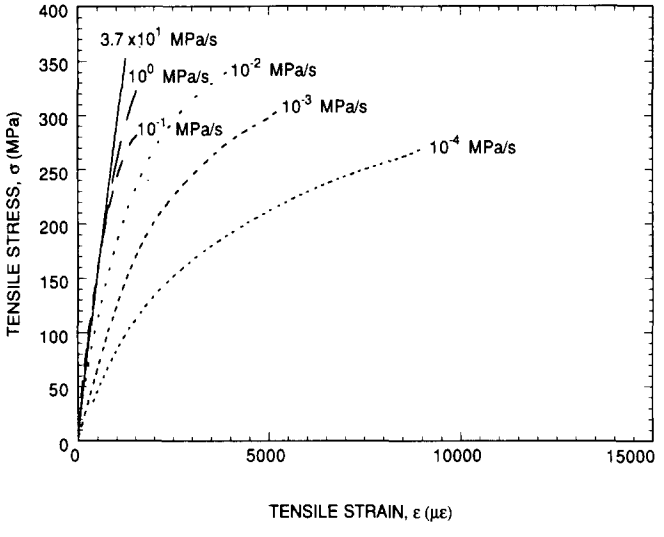

(b)

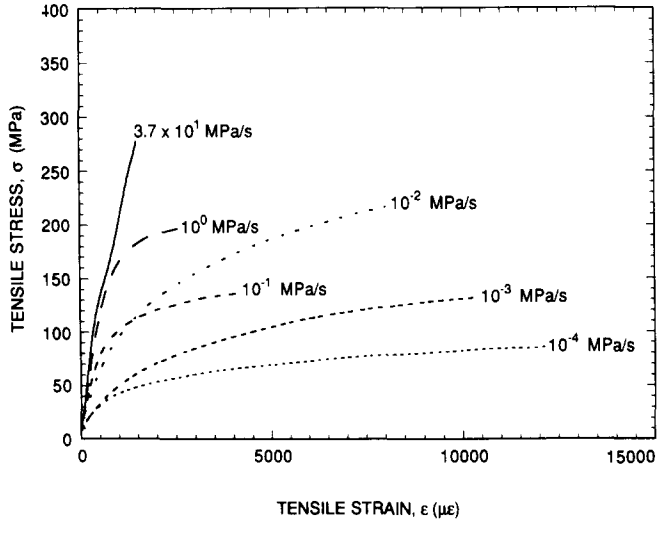

(c)

Fig. 4. Tensile stress–strain behavior of PY6 silicon nitride over a range of constant stress rates at temperatures: (a) 1150°C, (b) 1260°C and (c) 1370°C.

deformation was readily detected at 1260 and 1370°C at stress rates $\leq 10^{-2}$ MPa/s, as considerable nonlinearity in the stress–strain curves was present in this regime. Note that the nonlinearity increased with decreasing stress rate. This nonlinear deformation behavior might result from the ongoing accumulation of creep damage (cavities and microcracks) during dynamic fatigue testing. Moreover, the failure strains for the nonlinear stress–strain curves ($\leq 10^{-2}$ MPa/s) at 1260 and 1370°C were substantially greater than those for the linear stress–strain curves ($> 10^{-2}$ MPa/s) as shown in Fig. 5. No significant variation of the failure strains at all stress rates was observed at 1150°C.

The observed stress–strain relationship described can be qualitatively explained as follows. With the assumption that dynamic fatigue tests occur mainly in the first section of the primary creep range, a simplified relationship for stress and strain rates based on time hardening or strain hardening formulation can be obtained as:[27]

$$\dot{\varepsilon} \cong \frac{\dot{\sigma}}{E} + D\sigma^n \tag{5}$$

where $\dot{\varepsilon}$ is strain rate, E is Young's modulus, D is a constant at constant temperature, and n is the creep (or stress) exponent. Integration of eqn (5) generates the stress–strain relationship such that:

$$\varepsilon \cong \frac{\sigma}{E} + \frac{D\sigma^{n+1}}{(n+1)\dot{\sigma}} \tag{6}$$

Note that $\sigma = \dot{\sigma}t$ is applied for dynamic fatigue tests. The first term on the right-hand side (RHS) of eqn (6) is attributed to the instantaneous elastic response of material. The second term on the RHS of eqn (6) is related to the time dependence of creep processes. In the SCG-dominated regime, the second term on the RHS of eqn (6) is negligible or makes minor

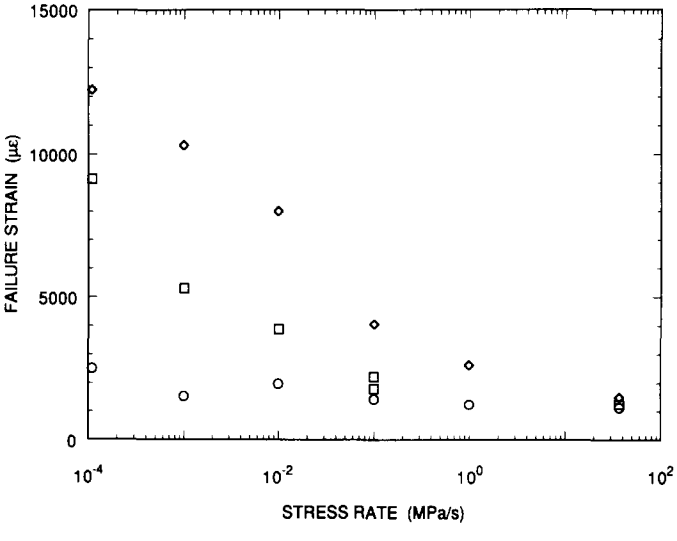

Fig. 5. Tensile failure strains of PY6 silicon nitride over a range of constant stress rates at (○) 1150, (□) 1260 and (◇) 1370°C.

contribution to the total strain, thereby generating linear stress–strain behavior (with a nearly identical slope) as observed at 1150°C as well as at high stress rates at 1260 and 1370°C. The minor deviation from linearity just prior to failure in these linear stress–strain curves possibly results in compliance changes due to subcritical crack growth of the failure-initiating flaw. Since Young's modulus did not decrease substantially in the SCG-dominated regime, the final failure strains at 1150°C as well as at high stress rates at 1260 and 1370°C are comparable.

In the creep-dominated regime, both terms on the RHS of eqn (6) would make significant contributions to the nonlinear stress–strain behavior observed for low stress rates at 1260 and 1370°C. Firstly, damage accumulation by formation and growth of creep cavities and microcracks could cause a decrease in Young's modulus (elastic creep) and lead to an apparent nonlinear stress–strain relationship.[28–30] Under certain conditions in some ceramics, the reduction in Young's modulus could be as much as a factor of 5.[28] Secondly, the nonlinear deformation from the second term on the RHS of eqn (6) could be attributed to creep processes related to diffusion, viscous flow, or other mechanisms or a combination of these. The second term on the RHS of eqn (6) also reveals the inverse relationship between stress rate and nonlinear strain; i.e. at a certain stress level reached during dynamic fatigue testing, low stress rates would generate more deformation than high stress rates. The experimental results did show this trend for the nonlinear stress–strain behavior present in the creep-dominated regime at low stress rates at 1260 and 1370°C. However, the first term on the RHS of eqn (6) is also implicitly associated with stress rate. The influence of stress rate on the intensity of formation and growth of creep cavities and microcracks would affect the extent of decrease in Young's modulus and adjunct nonlinear deformation. A quantitative analysis of each term on the RHS of eqn (6) which contributes to the nonlinear stress–strain behavior is not within the scope of this paper. Further research is needed for a rigorous treatment of this issue.

It is obvious from these dynamic fatigue results that SCG, crack blunting or healing, and creep damage generation can be competing processes at various stress rates in the temperature range of 1150 to 1370°C for this HIPed silicon nitride. It is likely that all these processes operate simultaneously but with one dominating over the others under certain conditions. SCG of pre-existing flaws controls the failures at all stress rates at 1150°C as well as at stress rates $>10^{-2}$ MPa/s at 1260 and 1370°C. However, failures for the cases with stress rates $\leq 10^{-2}$ MPa/s at 1260 and 1370°C were likely due to creep rupture. The increase in failure stress at 10^{-2} MPa/s at 1260 and 1370°C suggests that the localized defects responsible for failures at stress rate $>10^{-2}$ MPa/s are effectively blunted. Otherwise, the strength would continue to decrease with decreasing stress rate. Blunting may be due to internal oxidation (i.e. crack shape geometry effect) or relaxation of crack tip stress due to creep (i.e. stress effect).

3.4 Comparison of static and dynamic fatigue

Comparison of static and dynamic fatigue behavior of this HIPed silicon nitride at 1150, 1260 and 1370°C is shown in Fig. 6(a), (b) and (c), respectively, with maximum stress plotted versus time to failure. The maximum stress in these figures is equal to the applied constant stress and fracture strength for static and dynamic fatigue, respectively. The time to failure is the actual failure time in static fatigue, while in dynamic fatigue, it is the effective time to failure calculated using eqn (4) and the N values obtained in static fatigue.

In Fig. 6(a), the continuity in the data is illustrated by a single straight line through the static and dynamic fatigue results at 1150°C. It is implicit by this continuity that the failure mechanisms in static and dynamic fatigue at 1150°C are identical. SCG has been identified as the prevailing failure mechanism in static fatigue of this HIPed silicon nitride at 1150°C,[20] suggesting that SCG is also the governing failure mechanism for dynamic fatigue at 1150°C. Differences in the N values of 22 and 98 for static and dynamic fatigue tests, respectively, might be attributable to statistical variability. Even though only four and six failed specimens were used to evaluate the static and dynamic fatigue results, respectively, the agreement of the two test results as described by the single straight line in Fig. 6(a) demonstrates the dominance of SCG as the common failure mechanism.

At 1260 and 1370°C, all static and dynamic fatigue data could not be described by a single straight line, as shown in Fig. 6(b) and (c). Two straight lines were needed to reasonably fit all the data divided into two regions at each temperature. The effective dynamic fatigue failure times with stress rates $\leq 10^{-2}$ MPa/s were comparable with the static fatigue failure time regions on the right in Fig. 6(b) and (c), indicating the similarity of failure mechanisms between static fatigue and dynamic fatigue in this stress rate region. The description of the rest of dynamic fatigue data at either temperature by another straight line with different slope (regions on the left in Fig. 6(b) and (c)) implies a change of failure mechanism in dynamic fatigue for stress rates $>10^{-2}$ MPa/s at both 1260 and 1370°C. The failures of static fatigue specimens tested at 1260 and 1370°C were attributed to creep rupture.[20] Thus, creep rupture might be the dominant failure

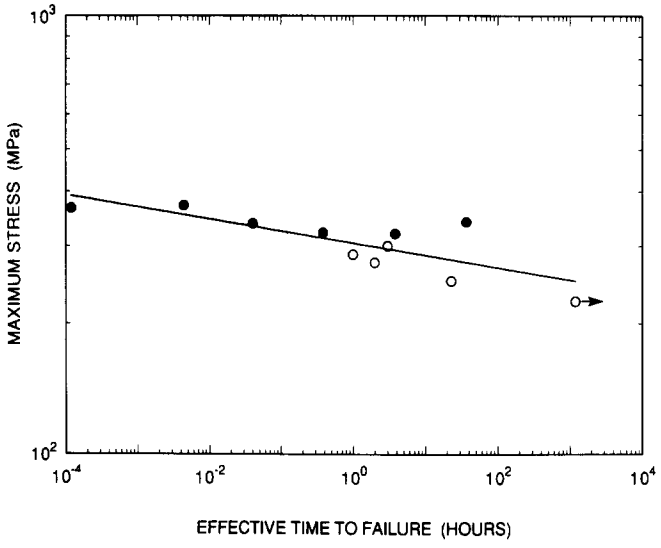

(a)

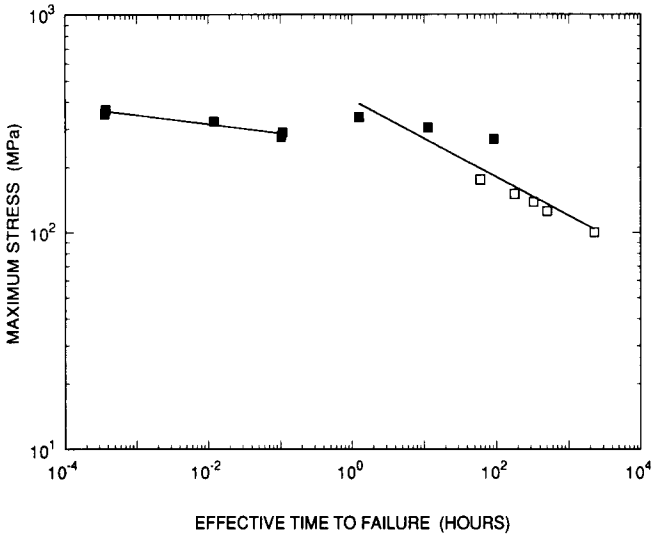

(b)

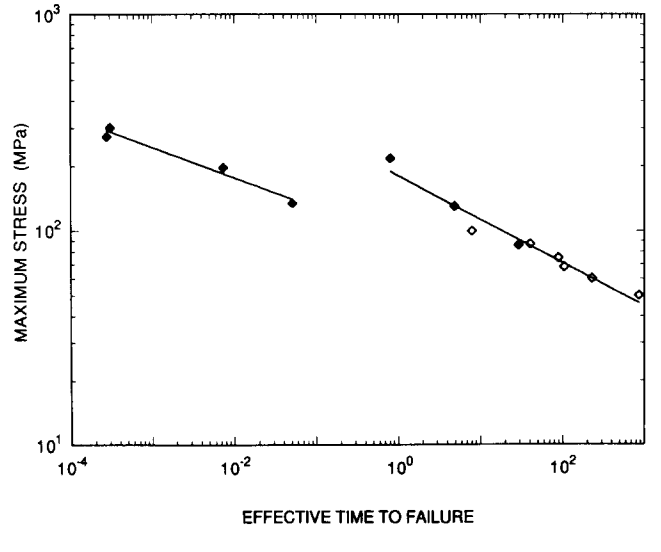

(c)

Fig. 6. Comparison of tensile static (○, □, ◇) and dynamic (●, ■, ◆) fatigue results of PY6 silicon nitride at temperatures: (a) 1150°C, (b) 1260°C and (c) 1370°C.

mechanism in dynamic fatigue with stress rates $\leq 10^{-2}$ MPa/s at 1260 and 1370°C. The controlling failure mechanism in dynamic fatigue at stress rates $> 10^{-2}$ MPa/s at either 1260 or 1370°C changed to SCG.

It might be argued that, unlike the results at 1370°C, all dynamic fatigue data at 1260°C (Figs 3 and 6(b)) could also be fitted by a single straight line instead of being separated in two regions. However, this argument could not be supported either by the previously described macroscopic stress–strain relations or by the microstructural analysis detailed in the following discussion. Note that the stress–strain curves at 1260°C (Fig. 4(b)) exhibited considerable nonlinearity for stress rates $\leq 10^{-2}$ MPa/s and remained nearly linear for stress rates $> 10^{-2}$ MPa/s. Fractographic analysis (details will be described in the following section) also indicated extensive creep cavities for stress rates $\leq 10^{-2}$ MPa/s and not for stress rates $> 10^{-2}$ MPa/s at 1260°C. In general, 1260°C can be described as a transition temperature for the change of the failure mechanism in dynamic fatigue from a single mechanism (SCG) to dual mechanisms (SCG or creep rupture, depending on stress rate).

The above comparisons of dynamic and static fatigue behavior at 1150, 1260 and 1370°C support the previous postulation on the failure mechanisms in dynamic fatigue of this HIPed silicon nitride at various stress rates. The failure mechanism in dynamic fatigue at 1150°C was nearly insensitive to stress rate and governed by SCG. At 1260 and 1370°C the failure mechanism in dynamic fatigue became more stress-rate dependent and dominated by SCG at stress rates greater than 10^{-2} MPa/s, and by creep rupture at stress rates $\leq 10^{-2}$ MPa/s.

Note that the failure life prediction method discussed previously is based on the assumption that static and dynamic fatigue failure mechanisms are identical and dominated by SCG of similar initial flaws to critical sizes. This assumption is valid in most ceramics at the temperatures where SCG is the major failure mechanism. For example, flexural tests of two sintered silicon nitride ceramics at 1000°C[9,12] revealed nearly identical values of N for static and dynamic fatigue in which the dominant failure mode was SCG. However, caution is advised in the application of this slow crack growth model to correlate static and dynamic fatigue behavior at elevated temperatures where creep processes and crack blunting can compete with SCG. The validity of using the linear-elastic fracture mechanics parameter, K_I, in the expression of crack growth rate needs to be examined. Other parameters such as C^*, the creep analogue to the J integral, may be considered in the description of crack growth rate as stress relaxation occurs around the crack tip due to

creep processes. Moreover, with the possibility of creep-assisted flaw/crack blunting or healing, creep processes could modify the flaw population initially present in material, thereby violating the fundamental basis of the SCG model that fatigue failure occurs by subcritical crack growth of pre-existing flaws. These possibilities explain why the correlation of tensile static and dynamic fatigue of PY6 in the present investigation could not be well defined by using only the slow crack growth model, particularly at temperatures $\geq 1260°C$. Other factors such as creep damage and crack blunting need to be implemented to refine the correlation between static and dynamic fatigue.

3.5 Slow crack growth versus creep rupture

Fractographic analysis of the failed fatigue specimens using scanning electron microscopy (SEM) is presented in this section. If two distinct regions of behavior exist in the dynamic fatigue at 1260 and 1370°C, then the fracture surfaces should look different when comparing regions. In fact, two different types of features were observed on the fracture surfaces of dynamic fatigue specimens at various stress rates. The first type of feature appeared as well-defined mirror, mist and hackle regions for all specimens tested at 1150°C as well as in those tested at stress rates $>10^{-2}$ MPa/s at 1260 and 1370°C (Fig. 7(a)). This is a typical fracture pattern for failures dominated by a SCG mechanism, which also appeared in the static fatigue specimens tested at 1150°C.[20] The second type of feature appeared as a transition to a small creep damage zone (region of high surface roughness) originating from the outer gage section surface (Fig. 7(b)). This feature was present for stress rates $\leq 10^{-2}$ MPa/s at both 1260 and 1370°C. This transition was more evident at 1370°C than at 1260°C. At 1370°C and 10^{-4} MPa/s (Fig. 7(c)) no hackle markings were present, suggesting that the true mirror size exceeded the specimen dimensions. The failures in these specimens are likely to have occurred as a result of the coalescence of creep damage followed by the nucleation and growth of creep cracks. Moreover, the accumulation process for creep damage appeared to originate from the outer surface where oxidation scale was created, thus suggesting the influence of oxidation in the damage coalescence stage for this HIPed silicon nitride. The presence of creep damage zones also occurred in the static fatigue specimens at 1260 and 1370°C.[20]

Detailed SEM examination of fracture origins and cavities along the fracture surfaces was restricted by the presence of an oxide scale created by exposure of the fresh fracture surface to ambient air at elevated temperature at the time of failure. However, a secondary fracture surface parallel to

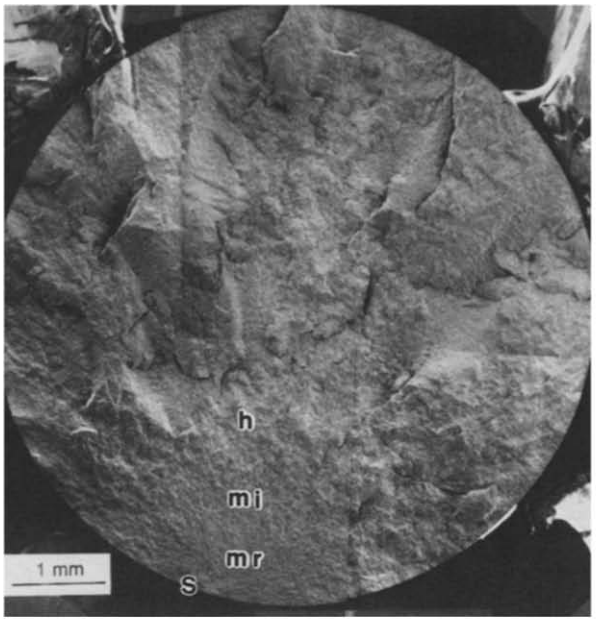

(a)

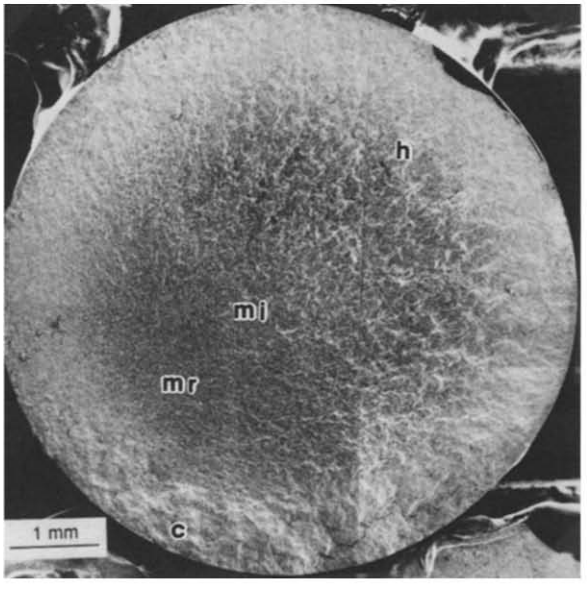

b)

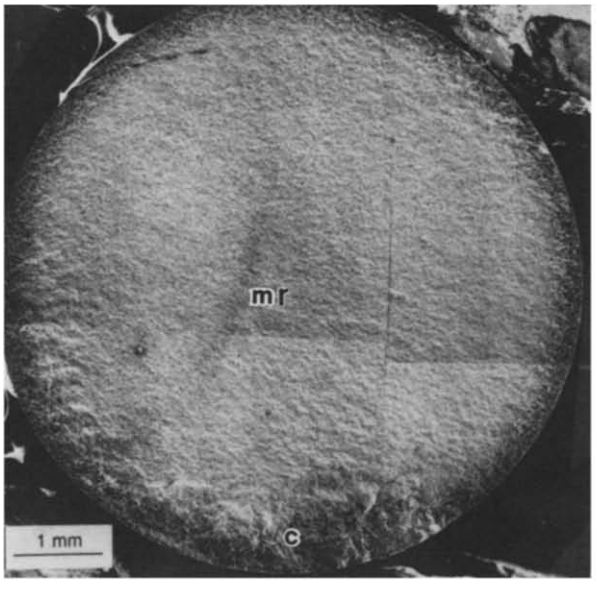

c)

Fig. 7. SEM micrographs of the typical fracture surfaces in dynamic fatigue specimens: (a) $3{\cdot}7 \times 10^{1}$ MPa/s at 1370°C, (b) 10^{-3} MPa/s at 1370°C and (c) 10^{-4} MPa/s at 1370°C (s: slow crack growth region; mr: mirror region; mi: mist region; h: hackle region; c: creep damage region).

the test fracture surface in the gage section was generated so as to expose possible creep damage. Fractographic analysis of static fatigue specimens[20] has indicated extensive cavitation along the two-grain boundaries throughout the gage section volume in static fatigue specimens tested at 1260 and 1370°C. No such extensive creep damage was found in static fatigue specimens tested at 1150°C. Absence of extensive creep cavities was also noted in dynamic fatigue specimens tested at 1150°C as well as in those tested at 1260 and 1370°C for stress rates $>10^{-2}$ MPa/s (Fig. 8(a)). In contrast, extensive creep cavities along the two-grain boundaries were observed in the dynamic fatigue specimens tested at stress rates $\leq 10^{-2}$ MPa/s at both 1260 and 1370°C (Fig. 8(b)). In the creep-dominated regime, cavity size increases with increasing temperature. This is presumably due to decreasing viscosity with increasing temperature. Furthermore, the creep-related damage might blunt and heal the initial defects and restrict their growth. This would explain why the fracture strength in the creep-dominated regime ($\leq 10^{-2}$ MPa/s) at 1260 and 1370°C was greater than the value extrapolated from the results from the SCG-dominated regime ($>10^{-2}$ MPa/s).

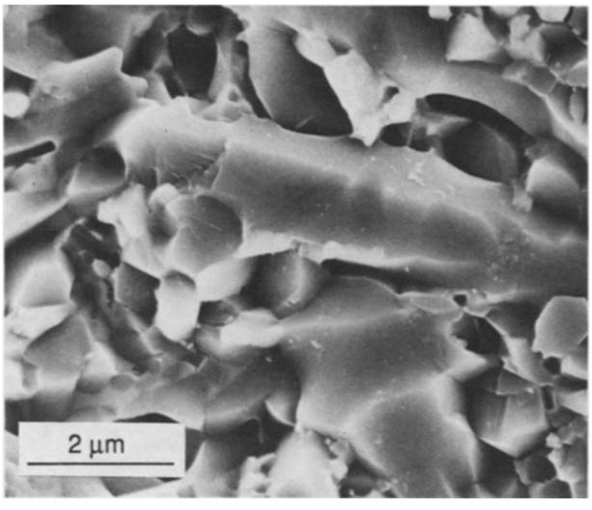

(a)

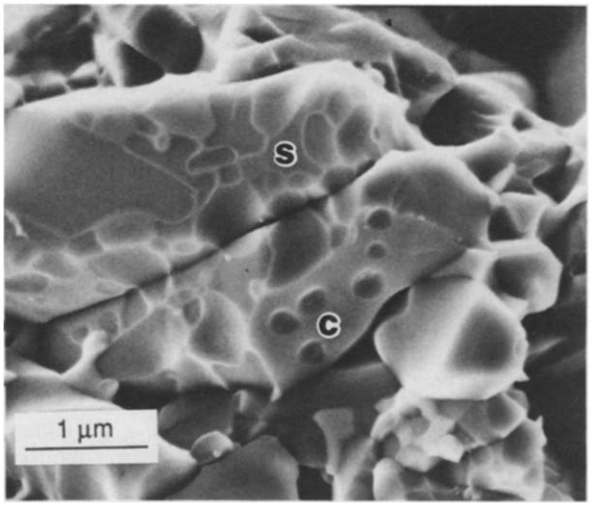

(b)

Fig. 8. High magnification SEM micrographs of secondary fracture surfaces: (a) $3{\cdot}7 \times 10^{1}$ MPa/s at 1370°C (without cavitation) and (b) 10^{-3} MPa/s at 1370°C (c: with cavities; s: skeletal pattern of boundary phase).

In general, the similarity of fracture surface features between dynamic and static fatigue specimens supports the argument that dynamic fatigue failures were also controlled by SCG at 1150°C as well as at stress rates $>10^{-2}$ MPa/s at 1260 and 1370°C, and governed by creep rupture at 1260 and 1370°C for stress rates $\leq 10^{-2}$ MPa/s. A comprehensive discussion of the creep damage morphology has been given in a previous study on creep properties of this silicon nitride.[20] A brief description of the cavitation morphology is presented as follows. As shown in Fig. 8(b), the cavities created along the two-grain boundaries are lenticular in shape. These cavities extended into the silicon nitride grains, suggesting that the growth mechanism involved solution/precipitation rather than viscous flow. Moreover, another common feature noticed on the secondary fracture surfaces for stress rates $\leq 10^{-2}$ MPa/s at 1260 and 1370°C was the skeletal pattern of the intergranular phase outlining the interfaces between small grain clusters and a single large grain (Fig. 8(b)). The formation of this pattern may have been a consequence of grain separation by viscous flow of the boundary phase. Such deformation would lower the local fracture resistance of the intergranular phase and provide a preferred failure path during secondary fracture. This viscous flow process would ultimately lead to the formation of facet-sized microcracks.[31,32] This microstructural evidence suggests that the primary mechanism in the creep deformation is grain-boundary diffusion accompanied by cavitation and grain separation by viscous flow.

The suppression of extensive creep cavitation in static and dynamic fatigue specimens at 1150°C possibly resulted from the increased viscosity of the intergranular phase. The inhibition of extensive creep damage (or creep strain) in dynamic fatigue for higher stress rates at 1260 and 1370°C occurred because the failure time by propagation of a single macrocrack was too short to allow any appreciable creep damage.

4 Conclusions

(1) Static and dynamic fatigue susceptibility of the tested HIPed silicon nitride increased with temperature in the range of 1150 to 1370°C.

(2) Comparison of effective time to failure and microstructural observations indicated that

static and dynamic fatigue results at 1150°C can be correlated to a SCG model.

(3) A transition in the dynamic fatigue failure mechanism from SCG to creep rupture appeared to occur at stress rates $\leq 10^{-2}$ MPa/s for 1260 and 1370°C. The existence of this transition is supported by macroscopic nonlinear stress–strain curves and microscopic fractographic evidence.

(4) Caution is advised in the application of the SCG model to correlate static and dynamic fatigue behavior in ceramics at elevated temperatures where creep processes and crack blunting can compete with SCG.

Acknowledgements

Research was performed at the High Temperature Materials Laboratory and sponsored by the US Department of Energy, Assistant Secretary for Conservation and Renewable Energy, Office of Transportation Technologies, as part of the Ceramic Technology Project of the Materials Development Program, under contract DE-AC05-84OR21400 with Martin Marietta Energy Systems, Inc. The authors thank Drs P. F. Becher and H. T. Lin for reviewing the manuscript.

References

1. Wiederhorn, S. M. & Fuller Jr, E. R., Structural reliability of ceramic materials. *Mater. Sci. Eng.*, **71** (1985) 169–86.
2. Helms, H. E., Johnson, R. A. & Groseclose, L. E., AGT 100-advanced gas turbine technology developed project. In *Proceedings of the Twenty-Third Automotive Technology Development Contractors' Coordination Meeting, Series Number P-165.* Society of Automotive Engineers, Warrendale, PA, 1986, pp. 137–55.
3. Carruthers, D. & Lindberg, L., Critical issues for ceramics for gas turbines. In *Third International Symposium on Ceramic Components and Materials for Engines*, ed. V. J. Tennery. American Ceramic Society, Westerville, OH, 1988, pp. 1258–72.
4. Yeckley, R. L. & Siebein, K. N., High temperature cavitation of HIP silicon nitride. In *Third International Symposium on Ceramic Components and Materials for Engines*, ed. V. J. Tennery. American Ceramic Society, Westerville, OH, 1988, pp. 751–65.
5. Quinn, G. D., Fracture mechanism maps for advanced structural ceramics. Part 1: Methodology and hot-pressed silicon nitride results. *J. Mater. Sci.*, **25** (1990) 4361–76.
6. Quinn, G. D., Fracture mechanism maps for advanced structural ceramics. Part 2: Sintered silicon nitride. *J. Mater. Sci.*, **25** (1990) 4377–92.
7. Chuck, L., Coodrich, S. M., Hecht, N. L. & McCullum, D. E., High-temperature tensile strength and tensile stress rupture behavior of Norton/TRW NT-154 silicon nitride. *Ceram. Eng. Sci. Proc.*, **11** (1990) 1007–27.
8. Foley, M. R. & Tressler, R. E., Threshold stress intensity for crack growth at elevated temperatures in a silicon nitride ceramic. *Adv. Ceram. Mater.*, **3** (1988) 382–6.
9. Chang, J., Khandelwal, P. & Heitman, P. W., Dynamic and static fatigue behavior of sintered silicon nitrides. *Ceram. Eng. Sci. Proc.*, **8** (1987) 766–77.
10. Ernstberger, U., Grathwohl, G. & Thümmler, F., High-temperature durability and limits of sintered and hot-pressed silicon nitride materials. *Int. J. High Tech. Ceram.*, **3** (1987) 43–61.
11. Bethge, D., High temperature creep and slow crack growth properties of HPSN as an example of ceramics containing a glassy phase. *Int. J. High Tech. Ceram.*, **3** (1987) 199–230.
12. Khandelwal, P. K., Chang, J. & Heitman, P. W., Slow crack growth in sintered silicon nitride. In *Fracture Mechanics of Ceramics*, Vol. 8, ed. R. C. Bradt, A. G. Evans, D. P. H. Hasselman & F. F. Lange. Plenum Press, NY, 1986, pp. 351–62.
13. Govila, R. K., Strength characterization of yttria-doped sintered silicon nitride. *J. Mater. Sci.*, **20** (1985) 4345–53.
14. Oda, I., Matsui, M. & Soma, T., High temperature fatigue failure in pressureless sintered silicon nitride. In *Progress in Nitrogen Ceramics*, ed. F. L. Riley. Martinus Nijhoff Publishers, Boston, 1983, pp. 501–6.
15. Kossowsky, R., Miller, D. G. & Diaz, E. S., Tensile and creep strength of hot-pressed Si_3N_4. *J. Mater. Sci.*, **10** (1975) 983–97.
16. Pasto, A. E., Van Schailkwyk, W. C. & Mahoney, F. M., Creep behavior of yttria- and alumina-doped silicon nitride. In *Third International Symposium on Ceramic Components and Materials for Engines*, ed. V. J. Tennery. American Ceramic Society, Westerville, OH, 1988, pp. 776–85.
17. Ferber, M. K., Tiegs, T. N. & Jenkins, M. G., Effect of post-sintering microwave treatments upon the mechanical performance of silicon nitride. *Ceram. Eng. Sci. Proc.*, **12** (1991) 1993–2004.
18. Tuersley, I. P., Leng-Ward, G. & Lewis, M. H., High-temperature Si_3N_4-based ceramics. *Brit. Ceram. Proc.*, **26** (1990) 231–46.
19. Xu, Y. R., Yen, T. S. & Fu, X. R., Grain boundary tailoring of high performance nitride ceramics and their creep property studies. In *Third International Symposium on Ceramic Components and Materials for Engines*, ed. V. J. Tennery. American Ceramic Society, Westerville, OH, 1988, pp. 739–50.
20. Ferber, M. K. & Jenkins, M. G., Evaluation of the creep-fatigue behavior of a HIPed silicon nitride. *J. Am. Ceram. Soc.*, **75** (1992) 2453–62.
21. Grathwohl, G., Current testing methods—a critical assessment. *Int. J. High Tech. Ceram.*, **4** (1988) 123–42.
22. Jenkins, M. G., Effect of bending of the room-temperature tensile strength structural ceramics. In *Proceedings of the VII International Congress on Experimental Mechanics.* Society for Experimental Mechanics, Bethel, CT, 1992, pp. 1171–8.
23. Wiederhorn, S. M., Subcritical crack growth in ceramics. In *Fracture Mechanics of Ceramics*, Vol. 2, ed. R. C. Bradt, D. P. H. Hasselman & F. F. Lange. Plenum Press, NY, 1974, pp. 623–46.
24. Ritter, J. E., Engineering design and fatigue failure of brittle materials. In *Fracture Mechanics of Ceramics*, Vol. 4, ed. R. C. Bradt, D. P. H. Hasselman & F. F. Lange. Plenum Press, NY, 1978, pp. 667–86.
25. McCullum, D. E., Hecht, N. L., Chuck, L. & Goodrich, S. M., Summary of results of the effects of environment on mechanical behavior of high-performance ceramics. *Ceram. Eng. Sci. Proc.*, **12** (1991) 1886–913.
26. Choi, S. R., Salem, J. A. & Gyekenyesi, J. P., Dynamic fatigue property of silicon carbide whisker-reinforced silicon nitride. *Ceram. Eng. Sci. Proc.*, **12** (1991) 1524–36.
27. Fett, T. & Munz, D., Determination of crack growth parameter N in ceramics under creep conditions. *J. Test. Eval.*, **3** (1985) 143–51.
28. Venkateswaran, A., Donaldson, K. Y. & Hasselman, D. P. H., Role of intergranular damage-induced decrease in Young's modulus in the nonlinear deformation and fracture

of an alumina at elevated temperatures. *J. Am. Ceram. Soc.*, **71** (1988) 565–76.
29. Hasselman, D. P. H., Venkateswaren, A. & Donaldson, K. Y., Contribution of damage by multiple crack growth to the strain-rate sensitivity of a polycrystalline alumina at elevated temperatures. *J. Mater. Sci.*, **24** (1989) 671–80.
30. Suresh, S. & Brockenbrough, J. R., A theory for creep by interfacial flaw growth in ceramics and ceramic composites. *Acta Metall. Mater.*, **38** (1990) 55–68.
31. Evans, A. G. & Rana, A., High temperature failure mechanisms in ceramics. *Acta Metall.*, **28** (1980) 129–41.
32. Tsai, R. L. & Raj, R., Creep fracture in ceramics containing small amounts of a liquid phase. *Acta Metall.*, **30** (1982) 1043–58.